environments

MDPI

*Article*

# Physicochemical Controls on Depth-Dependent Nutrient Mobility in the Intertidal Flat of a Coastal Lagoon

**Abdoulkader Moussa Siddo [1] and Katsuaki Komai [2,*]**

[1] Graduate School of Engineering, Kitami Institute of Technology, 165 Koen-cho, Kitami 090-8507, Hokkaido, Japan; d3237180040@std.kitami-it.ac.jp
[2] Division of Civil and Environmental Engineering, Kitami Institute of Technology, 165 Koen-cho, Kitami 090-8507, Hokkaido, Japan
* Correspondence: komai@mail.kitami-it.ac.jp

**Abstract**

In this study, we investigated how porewater salinity, temperature, ionic strength, and nutrient behavior vary with depth in the intertidal flats of Lake Komuke, a coastal lagoon in northern Japan. A central feature of this work is the use of nutrient activity and activity coefficients—thermodynamic parameters that more directly represent ion mobility—rather than concentrations alone. Statistical analyses showed that salinity exhibited clear depth-dependent variation and was the primary factor associated with changes in nutrient behavior, whereas temperature showed minimal variation and no detectable effect. Physicochemical modeling using the Pitzer approach demonstrated that increases in salinity and ionic strength with depth led to reductions in the activity coefficients of $NO_3^-$, $NH_4^+$, and $PO_4^{3-}$, with $PO_4^{3-}$ showing the greatest sensitivity due to its trivalent charge. Nutrient activities displayed contrasting vertical patterns: $NO_3^-$ and $NH_4^+$ tended to increase with depth, whereas $PO_4^{3-}$ exhibited a peak at −20 cm followed by lower values at deeper, more saline layers. These results indicate that subsurface nutrient mobility in coastal tidal flats is shaped primarily by ionic strength-driven non-ideal behavior and associated geochemical gradients. The findings provide baseline information for understanding nutrient dynamics in brackish sediments and support the improved assessment of subsurface biogeochemical processes in intertidal ecosystems.

**Keywords:** activity coefficient; activity; depth salinity; intertidal flat; ionic strength; nutrients

## 1. Introduction

Tidal flats are important ecosystems that can be found throughout the world. They are defined as dynamic zones between high and low tides [1–3] that play critical roles in nutrient cycling, carbon storage, and the survival of diverse organisms. In recent years, tidal flats have also been increasingly recognized as contributors to coastal blue carbon storage because their nutrient regeneration and organic matter decomposition processes influence carbon retention or release in sediments. Understanding these biogeochemical processes requires not only concentration-based evaluations but also thermodynamic parameters such as ion activity, which more directly describe nutrient mobility in sediment porewater. Tidal flats serve essential ecological roles as habitats for diverse species [3–6] and function as nutrient cycling hotspots [7–9]. Intertidal flats also act as a key interface between land and ocean [10], driving major biogeochemical processes, including dissolved inorganic nitrogen (DIN) and phosphorus (DIP) cycling [11], which support ecosystem productivity [12]. Because nutrient cycling is tightly coupled with organic matter mineralization,

Check for updates

Academic Editor: Meilin Wu

Received: 7 December 2025
Revised: 5 February 2026
Accepted: 9 February 2026
Published: 18 February 2026

**Copyright:** © 2026 by the authors. Licensee MDPI, Basel, Switzerland. This article is an open access article distributed under the terms and conditions of the Creative Commons Attribution (CC BY) license.

these processes are also linked to carbon dynamics and may influence whether tidal flats function as net sources or sinks of carbon over seasonal to annual timescales. The intertidal flat of Lake Komuke in northeastern Hokkaido, Japan, hosts numerous migratory bird species (170 to 180 species annually). Nutrient concentrations in this system are influenced by environmental factors, especially salinity and temperature, that vary with climatic and tidal conditions. Similar to the Wadden Sea, where tidal flats play a central role in coastal biogeochemical functioning [13], the tidal flats along the Sea of Okhotsk—including Lake Komuke—are expected to provide comparable ecological services in high-latitude environments. Understanding their biogeochemical dynamics is therefore crucial for maintaining ecological health in this region. In coastal lagoons such as Lake Komuke, low-salinity water derived from snowmelt and river inflow commonly overlies deeper saline porewater associated with salt wedge intrusion. This density-driven structure can generate steep vertical gradients in porewater salinity and geochemistry, providing a physical context for understanding depth-dependent nutrient mobility.

Salinity strongly regulates nutrient cycling through its effects on microbes, ionic interactions, and nutrient mobility. Microbial processes such as nitrification and denitrification can be altered by salinity fluctuations [14–16], and high salinity levels often inhibit microbial activity, reducing nutrient transformation rates [17–19]. In addition, a high ionic strength promotes ionic exchange among dissolved ions, modifying the availability of nitrogen and phosphorus species [20–24]. Salinity also influences nutrient mobility; for instance, $PO_4^{3-}$ desorbs more readily under high-ionic-strength environments, becoming more mobile in porewater [25,26]. These salinity-driven changes in nutrient mobility can alter both the intensity and spatial pattern of organic matter mineralization, thereby influencing the vertical distribution of carbon decomposition and storage in tidal flat sediments.

Temperature strongly influences microbial activity and organic matter decomposition [27,28]. Higher temperatures accelerate mineralization and increase the release of phosphorus and nitrogen after remineralization [29]. Extremely high or low temperatures can suppress nitrification [30], while warming reduces oxygen solubility and promotes anaerobic conditions that favor denitrification and the depletion of nitrogen and sulfate [31]. Conversely, aerobic conditions enhance nitrification and the regeneration of nitrate [32–34]. Temperature-driven variations in oxygen availability also influence $PO_4^{3-}$ retention through iron oxide formation [35]. Collectively, these processes determine whether organic matter is preserved in sediments or remineralized, linking thermal conditions to blue carbon retention.

Previous studies have evaluated tidal flat biogeochemistry using porewater chemistry [10,36–38], microbial analyses of nitrification and denitrification pathways [39,40], long-term monitoring of nutrients and environmental factors [41], and numerical simulations that capture nutrient exchange between porewater and the water column [42,43]. Despite these advances, key uncertainties remain regarding how depth-dependent changes in salinity and temperature regulate nutrient mobility and subsurface carbon cycling in intertidal sediments. Such gaps are particularly evident in understudied systems like Lake Komuke.

Thus, this study investigates how salinity and temperature variations influence nutrient mobility in tidal flat porewater to a depth of −40 cm along a 320 m transect. Porewater was sampled at −10 cm intervals to determine nutrient activities and activity coefficients for $NO_3^-$, $NH_4^+$, and $PO_4^{3-}$ together with salinity and temperature. By correlating nutrient behavior with these environmental gradients, we aim to clarify how physicochemical conditions regulate nitrogen and phosphorus mobility in intertidal sediments. This study offers basic insight into how depth-dependent physicochemical conditions influence the remineralization of organic matter and the behavior of inorganic nutrients in intertidal sediments.

Specifically, the following research questions are articulated:

(i) How does porewater salinity variation affect the ionic strength and ionic activity of nutrients such as $NO_3^-$, $NH_4^+$, and $PO_4^{3-}$ in intertidal flat sediments? (ii) Is temperature the most significant controller of the activity coefficient of $NO_3^-$, $NH_4^+$, and $PO_4^{3-}$ or salinity? (iii) Does nutrient concentration accurately represent actual nutrient behavior in brackish porewater without considering ionic strength-driven activity coefficients and activity?

Consequently, the following hypotheses are developed to empirically assess the robustness and limitations of classical interpretations of nutrients in past research on porewater nutrients, without claiming to invent a new method for nutrient mobility:

(i) Surface and subsurface porewater layers exhibit distinct ionic strength regimes driven primarily by salinity intrusion, producing depth-dependent gradients in nutrient activities. (ii) Temperature may modulate ionic interactions to a limited extent, but salinity-driven changes in ionic strength are expected to be the dominant factor controlling the activity coefficients of $NO_3^-$, $NH_4^+$, and $PO_4^{3-}$. (iii) Nutrient processes in saline porewater are better represented by the ionic strength-driven activity coefficient and activity rather than simple molar concentrations.

## 2. Materials and Methods

### *2.1. Study Area*

Lake Komuke is a coastal lagoon located in the northeast of Hokkaido, Japan. The lagoon consists of three interconnected basins, of which the first lake is linked to the Sea of Okhotsk through an artificial channel, forming a tidal flat due to the alternation of high and low tides. This study concentrated on the primary lake, the largest one, where tidal fluctuations directly influence sediment porewater. Sampling stations were arranged along a 320 m cross-shore transect (Figure 1).

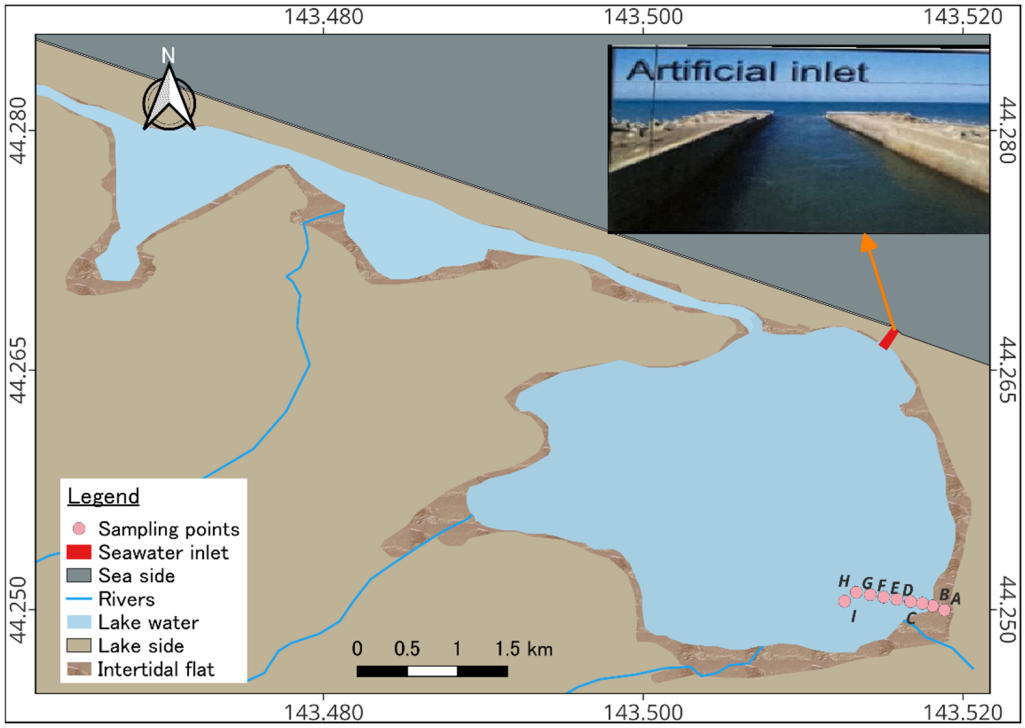



**Figure 1.** Panoramic view of Lake Komuke and sampling point locations.

### *2.2. Sampling Procedure*

Porewater samples were collected at nine stations during late spring and summer (19 May, 19 June, 21 July, and 23 August 2015). Using syringes attached to buried tubes, porewater was extracted from depths of −10, −20, −30, and −40 cm. The 0 cm sample represents the overlying surface water immediately above the sediment–water interface and serves as a reference layer for evaluating depth-dependent changes in porewater chemistry. Samples were filtered through cellulose mixed-ester filters to remove suspended solids before analysis. Concentrations of $NO_3^-$, $NH_4^+$, and $PO_4^{3-}$ were determined using a standard spectrophotometric colorimetric method using a continuous-flow analyzer (QuAAtro, SEAL Analytical, Mequon, WI, USA). Salinity and temperature at each depth were measured in situ during porewater extraction on the same scale. These measurements provide the basis for assessing how environmental gradients influence nutrient activity and activity coefficients. Although sampling covered late spring to summer, the primary objective of this study was to evaluate depth-dependent physicochemical controls on nutrient behavior within the sediment. Therefore, seasonal variability was not treated as an analytical factor; instead, all samples were interpreted collectively to characterize vertical patterns in geochemistry. The redox conditions and indicators (redox potential, dissolved oxygen, $Fe^{2+}/Fe^{3+}$, and sulfides) were not directly measured in situ; instead, they were used as inferential indicators of depth-related nutrient distributions within well-known geochemical frameworks.

### *2.3. Statistical Analysis*

A statistical analysis was performed to verify whether salinity and temperature showed systematic depth-dependent patterns across stations because these environmental variables form the background context for interpreting ionic strength variation. To evaluate such depth-related differences, we applied the Friedman test [44]. This test was selected as a nonparametric alternative to two-way ANOVA because the environmental variables and associated measurements did not satisfy the assumptions of normality and homogeneity of variance [45]. The Friedman test is particularly suitable for repeated-measures designs, where multiple depth-dependent observations are collected from the same stations under varying environmental conditions. Thus, salinity showed a statistically significant depth-dependent variation and was therefore investigated from a physicochemical and thermodynamic perspective to interpret nutrient ionic activity behavior with respect to depth. The statistical test of temperature showed no significant depth-related differences and was therefore not considered a potential controlling factor. Importantly, the test was used solely to confirm depth-related variation in salinity and temperature and was not intended to infer causal relationships with nutrient ionic activity.

### *2.4. Physicochemical Analysis*

#### 2.4.1. Ionic Strength

By definition, ionic strength is determined from the concentration of ions and their respective valence charge. Equation (1) shows the well-known thermodynamic formulation of ionic strength:

$$I = \frac{1}{2}\sum C_i Z_i^2 \quad (1)$$

where $I$ is the ionic strength, $C_i$ is the concentration of the ion, and $Z_i$ is the charge of the ion.

Equation (2) [46] does not replace the thermodynamic definition of ionic strength given in Equation (1), but is used here as an empirical proxy under brackish conditions where major ions dominate and salinity is strongly correlated with ionic strength. This approach

is adopted for practical reasons, as the full ionic speciation of porewater is difficult to determine in natural sediments.

$$I = \frac{19.924S}{1000 - 1.005S} \quad (2)$$

where S is the salinity. The coefficients originated from IUPAC 2013 atomic weights [47]. This expression is appropriate because salinity in the tidal flat results from seawater intrusion and better represents the physicochemical conditions of brackish porewater than concentration-based formulations.

#### 2.4.2. Activity and Activity Coefficient

Ion activity ($a_i$) was computed as follows:

$$a_i = \gamma_i.[c] \quad (3)$$

where $\gamma_i$ is the activity coefficient and [c] is the concentration. Because porewater ionic strength frequently exceeds levels where ideal behavior can be assumed, we used the Pitzer model [48] to estimate the activity coefficient of $NO_3^-$, $NH_4^+$, and $PO_4^{3-}$. The Pitzer formulation accounts for binary and ternary ion interactions and is widely applied to natural waters with elevated salinity.

In this study, the model was used not to refine thermodynamic parameters, but to provide a consistent framework for evaluating how salinity-driven changes in ionic strength modify nutrient behavior at depth. Parameter sets for the ion pairs relevant to $NO_3^-$, $NH_4^+$, and $PO_4^{3-}$ were adopted from Millero & Pierrot [49] and the related literature.

Thus, it is important to note that, in this study, ternary interaction parameters were not explicitly included due to the limited availability of reliable experimental data for nutrient-related ternary systems. This simplification may introduce uncertainty in the absolute values of activity coefficients, particularly under high-ionic-strength conditions; however, it does not affect the relative depth-dependent trends that are the primary focus of this study. Specifically, $PO_4^{3-}$ activity was evaluated as a computable thermodynamic species within the Pitzer framework. Although $PO_4^{3-}$ in natural seawater and brackish porewater is predominantly present as $HPO_4^{2-}$ under typical pH conditions, $PO_4^{3-}$ was used here as a thermodynamic reference to examine relative changes.

The full equations and coefficients used in the computation are presented in the Appendix A.

## 3. Results

### *3.1. Physicochemical Analysis of Porewater*

#### 3.1.1. Salinity as a Function of Ionic Strength

Salinity was measured in the tidal flat porewater, ranging from 0 to −40 cm (Figure 2a). Salinity increased with depth at most stations, reflecting the intrusion of seawater into the subsurface layer. Ionic strength was calculated from mean salinity values using Equation (2). As shown in Figure 2b, ionic strength increased linearly with salinity, indicating a strong correlation between these parameters. Thus, both salinity and ionic strength followed similar depth-dependent trends. The mean salinity was obtained from the field survey conducted in May, June, July, and August 2015, as shown in the Supplementary Materials (Figure S1).

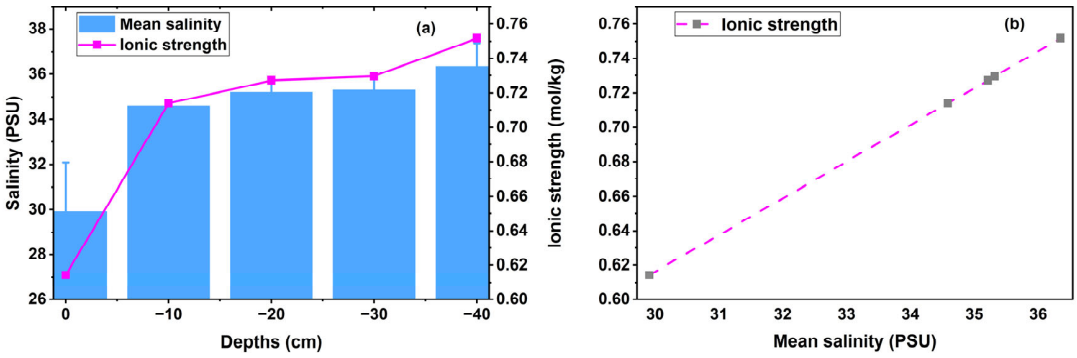



**Figure 2.** (**a**) Depth-dependent variations in porewater salinity and calculated ionic strength. Bar height indicates mean values across nine sampling stations, and error bars represent standard deviations. (**b**) Salinity-based calculation of ionic strength used for activity analysis.

### 3.1.2. Activity Coefficient of Ions in Porewater

The activity coefficients of $NO_3^-$, $NH_4^+$, and $PO_4^{3-}$ were calculated as a function of ionic strength (Figure 3). As ionic strength increases, the activity coefficients of all three ions decreased, consistent with non-ideal behavior in saline media. Over the observed ionic strength range (0.61–0.75 mol/kg), the activity coefficient of $NH_4^+$ decreased slightly from 0.624 to 0.623 and the activity coefficient of $NO_3^-$ decreased from 0.532 to 0.527. Meanwhile, the activity coefficient of $PO_4^{3-}$ showed a pronounced reduction from $3.7 \times 10^{-5}$ to $1.4 \times 10^{-5}$, which is consistent with values reported for trivalent phosphate species in high-ionic-strength natural waters, where activity coefficients on the order of $10^{-5}$ to $10^{-4}$ have been reported (e.g., $2.4 \times 10^{-5}$–$3.3 \times 10^{-5}$ in [49]; $<10^{-5}$ in [50]).

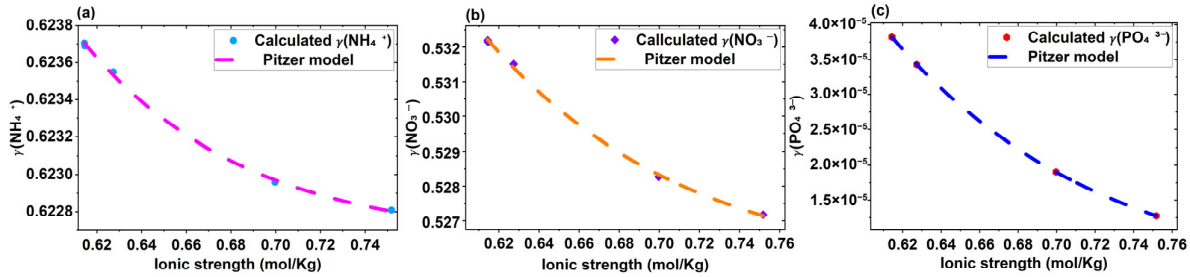



**Figure 3.** Correlation between ionic strength and activity coefficient (γ) of (**a**) $NH_4^+$, (**b**) $NO_3^-$, (**c**) $PO_4^{3-}$. Dashed lines represent activity coefficients estimated by the Pitzer model.

Depth profiles for activity coefficients (Figure 4) showed that values for $NO_3^-$, $NH_4^+$, and $PO_4^{3-}$ were nearly constant in the upper layer (around 0 cm to −10 cm), and then gradually decreased toward −40 cm. At −40 cm, the activity coefficients of $NO_3^-$ and $NH_4^+$ were slightly lower (0.527 and 0.622, respectively), while the activity coefficient of $PO_4^{3-}$ declined to $1.5 \times 10^{-5}$. This depth-dependent decrease is consistent with increasing ionic strength and enhanced ion–ion interaction in deeper, more saline porewater.

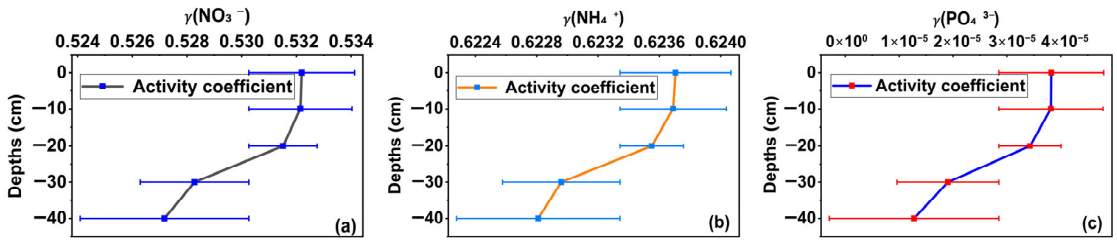



**Figure 4.** Vertical profiles of (**a**) $NO_3^-$, (**b**) $NH_4^+$, (**c**) $PO_4^{3-}$ activity coefficients (γ). Symbols indicate mean values across nine sampling stations, and error bars represent standard deviations.

3.1.3. Ionic Activity of Nutrients in Porewater

Nutrient ionic activity (molality-based) exhibited depth-dependent patterns (Figure 5). For $NO_3^-$, activity rose from 7.38 × $10^{-6}$ mol/kg at 0 cm to 47.9 × $10^{-6}$ mol/kg at −20 cm. A slight decrease occurred between −20 and −30 cm, followed by an increase to 57.7 × $10^{-6}$ mol/kg at −40 cm. However, $NO_3^-$ concentrations in all porewater samples were extremely low and often close to the analytical detection limit. Therefore, the apparent increase in $NO_3^-$ activity at deeper layers should be interpreted with caution, as the magnitude of this variation is comparable to analytical uncertainty and may not indicate a true geochemical trend in strongly reducing sediments. $NH_4^+$ activity increased markedly from 7.16 × $10^{-4}$ mol/kg at 0 cm to 5.8 × $10^{-2}$ mol/kg at −20 cm. It decreased slightly between −20 and −30 cm, then rose again to 7.0 × $10^{-2}$ mol/kg at −40 cm. $PO_4^{3-}$ activity increased from 4.0 × $10^{-9}$ mol/kg at 0 cm to 3.55 × $10^{-8}$ mol/kg at −20 cm, and then declined to 2.66 × $10^{-8}$ mol/kg at −40 cm.

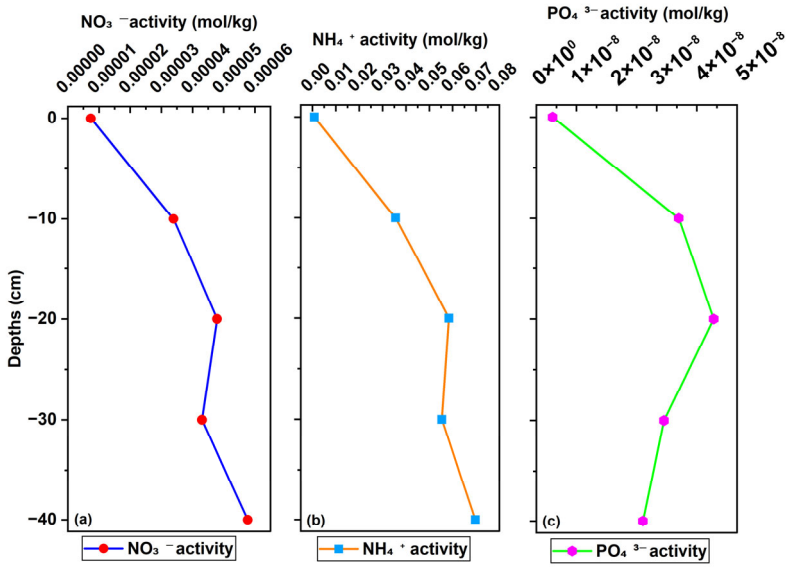



**Figure 5.** Vertical profiles of (**a**) $NO_3^-$, (**b**) $NH_4^+$, (**c**) $PO_4^{3-}$ activity.

The measured sediment porewater concentrations of $NO_3^-$, $NH_4^+$, and $PO_4^{3-}$ during the May–August study campaign at five sediment depths (0, −10, −20, −30, and −40 cm) are presented in the Supplementary Materials (Figure S2). The vertical distribution of nutrient concentration (mol/L) over the four months was determined and correlated with ionic activity, as shown in Figure 6. Additionally, Figures S3–S5 in the Supplementary Materials display the correlation between concentration and the ionic activity of $NO_3^-$, $NH_4^+$, and $PO_4^{3-}$ across the nine stations.

Figures 7–10 further illustrate the depth-dependent behavior of nutrient ionic activity and activity coefficients. Figure 7 shows that $NO_3^-$ activity increases with depth despite the decrease in its activity coefficient, indicating that concentration-driven effects dominate under a higher ionic strength. Given the low absolute concentrations noted above, however, this trend should be interpreted conservatively. Figure 8 demonstrates a pronounced increase in $NH_4^+$ activity at deeper layers, with a slight mid-depth depression suggesting a transition in redox conditions. Figure 9 highlights a distinct phosphorus pattern, where $PO_4^{3-}$ activity peaks at −20 cm and declines at deeper layers. Figure 10 summarizes the vertical profiles of ionic strength, showing positive correlations for $NO_3^-$ and $NH_4^+$ activity but a non-monotonic response for $PO_4^{3-}$. These plots collectively clarify how salinity and ionic strength gradients shape nutrient mobility across sediment depth.

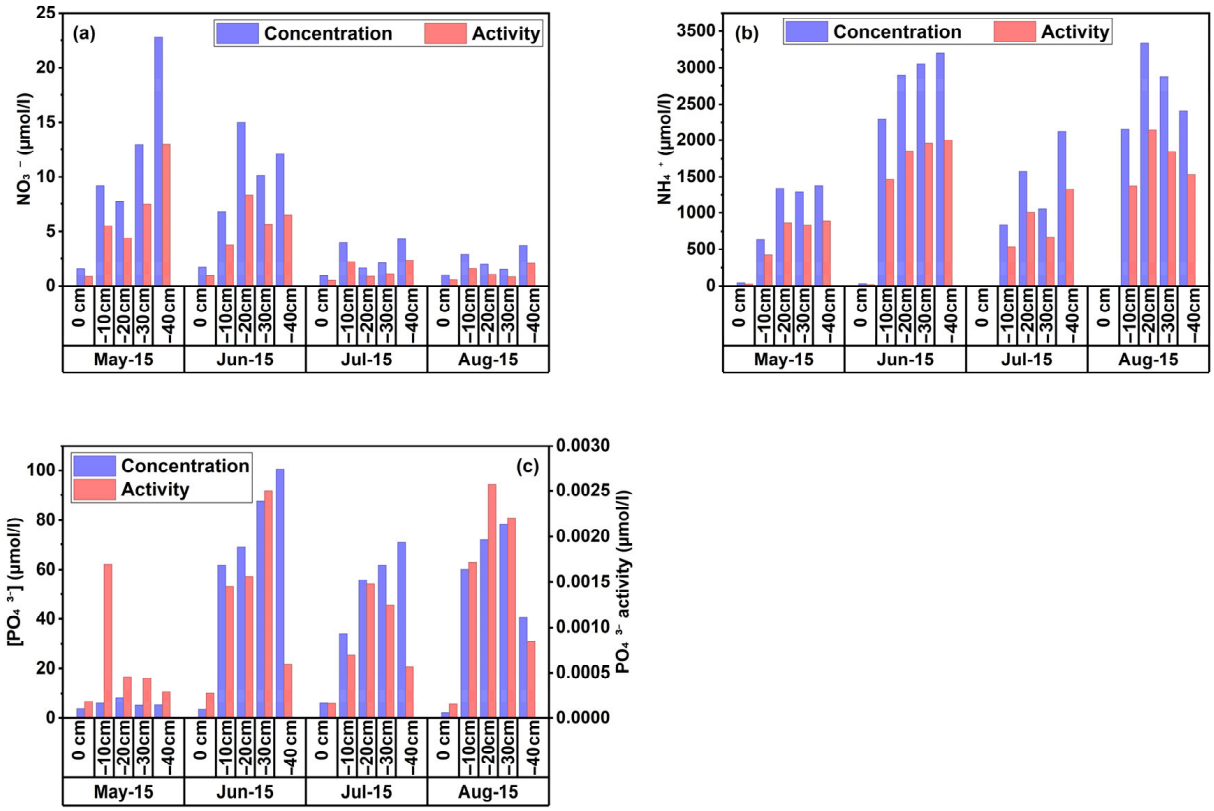



**Figure 6.** Monthly variations in porewater concentrations correlated with activity of (**a**) $NO_3^-$, (**b**) $NH_4^+$, (**c**) $PO_4^{3-}$ at different sediment depths.

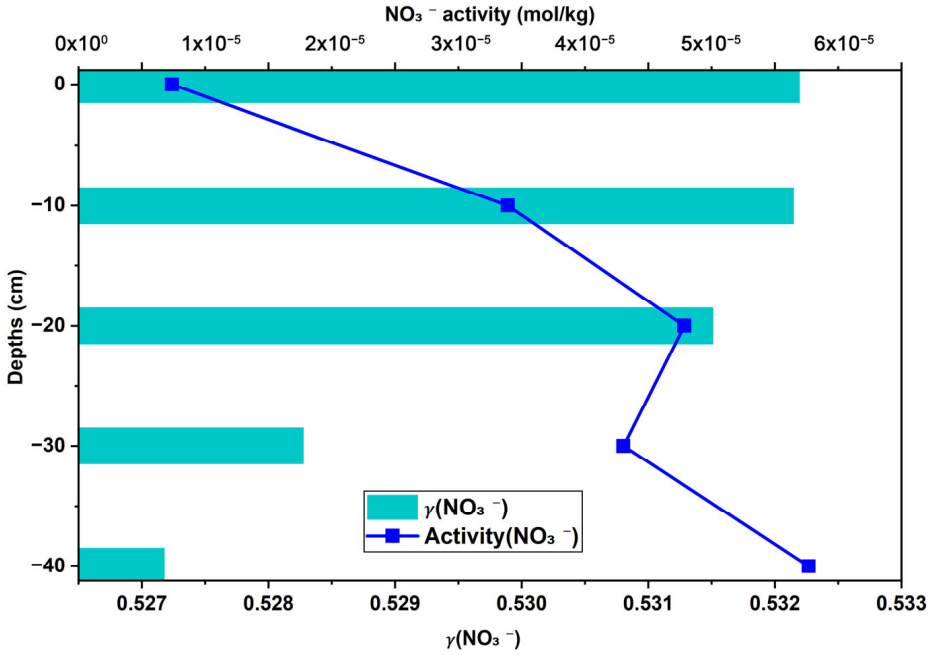



**Figure 7.** Vertical profiles of $NO_3^-$ activity and its activity coefficient γ.

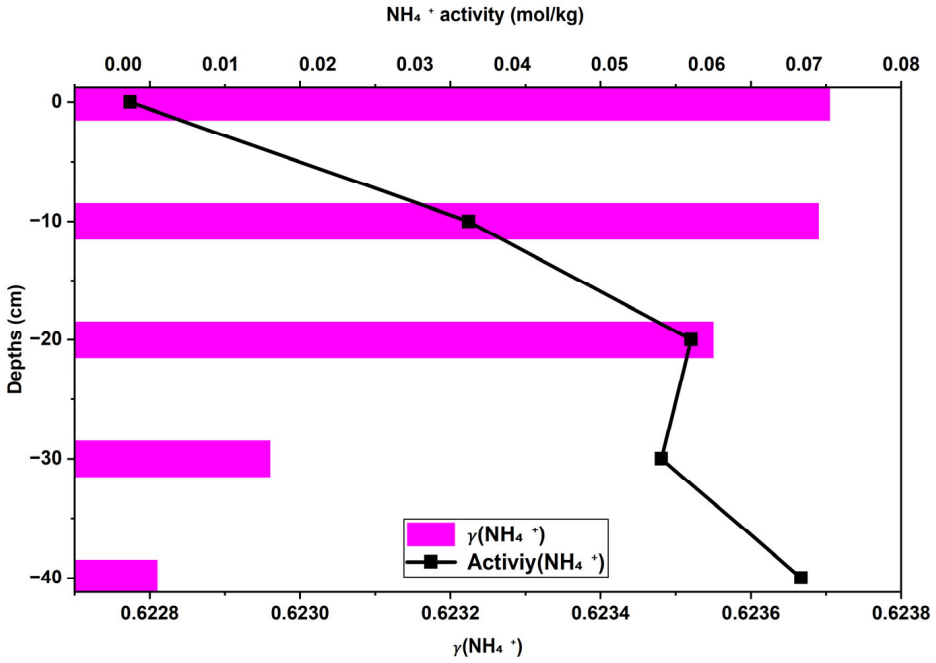



**Figure 8.** Vertical profiles of $NH_4^+$ activity and its activity coefficient γ.

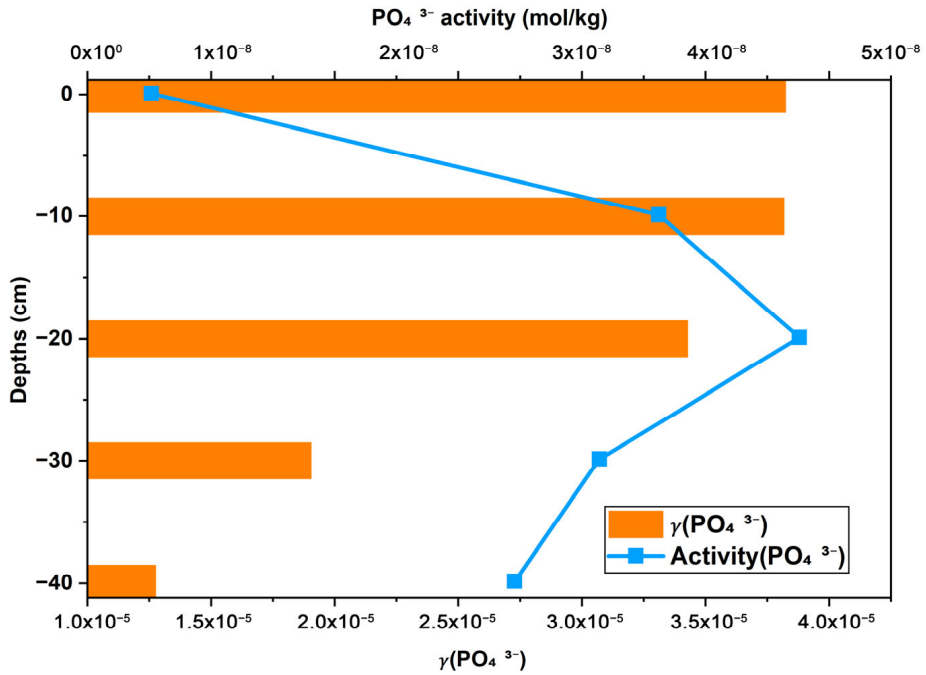



**Figure 9.** Vertical profiles of $PO_4^{3-}$ activity and its activity coefficient γ.

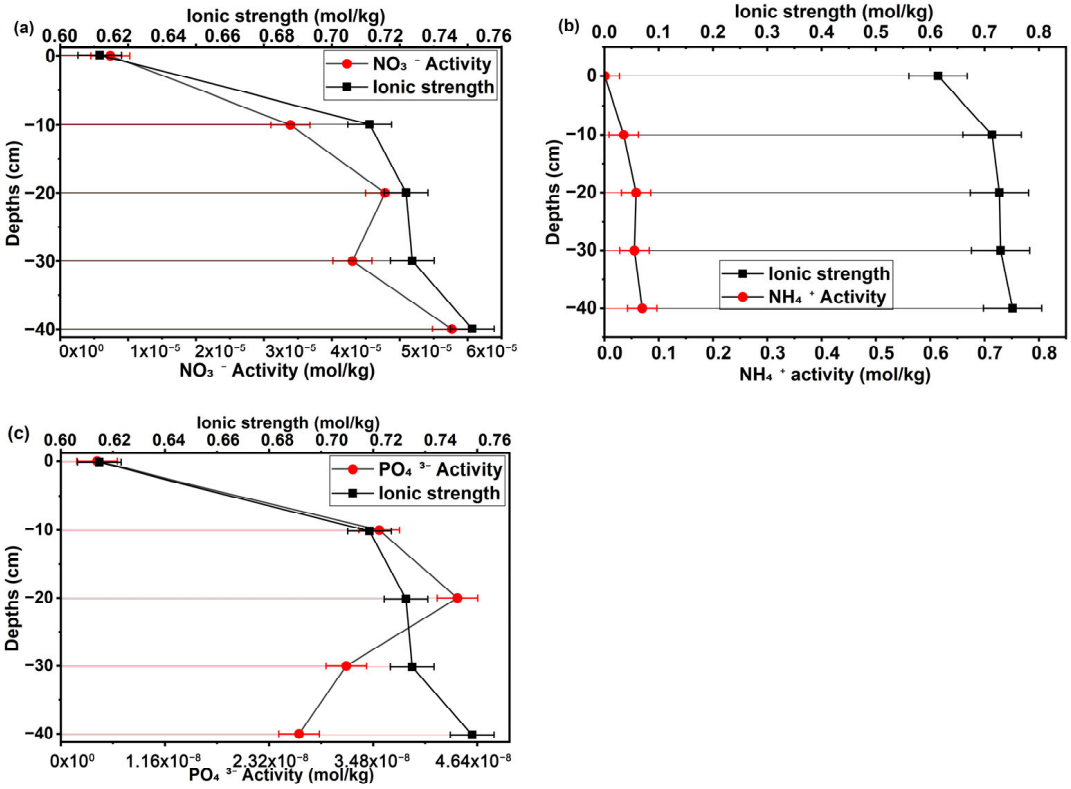



**Figure 10.** Vertical profiles of ionic strength and activities of (**a**) $NO_3^-$, (**b**) $NH_4^+$, (**c**) $PO_4^{3-}$ across sediment depth.

### *3.2. Statistical Analysis of Environmental Controls*

The Friedman test was applied to examine whether salinity and temperature differed systematically among the five sampling depths across the nine stations. This analysis was used to identify depth-dependent environmental gradients that may influence porewater biogeochemistry (Table 1). A significance threshold of $p = 0.05$ (95% confidence level) was applied.

**Table 1.** Friedman's test results for salinity and temperature across the different depths.

| Variables | Treatments (Depths in cm) | Degree of Freedom | Test Statistical $F_r\ \chi(8)$ | F-Critical | *p*-Value |
|---|---|---|---|---|---|
| Salinity | 5 | 4 | 13.33 | 9.49 | 0.00976 * |
| Temperature | 5 | 4 | 2.31 | 9.49 | 0.6787 |

*: $p < 0.05$.

Salinity showed a statistically significant difference among depths ($p < 0.05$), whereas temperature did not. These findings indicate that depth-related environmental gradients are primarily driven by salinity rather than temperature during the study period.

Because salinity varied significantly, a post hoc Dunn's test with Bonferroni's correction was conducted (Table 2). The pairwise comparison revealed that the difference between 0 cm and −20 cm was significant, with a mean effect size of W = 0.37, while no other depth pairs showed significant differences.

**Table 2.** Dunn's pairwise comparison of depth salinity and adjusted *p*-value using Bonferroni's correction.

| Depths Pairwise Comparison | Test Statistic | Standard Test Statistic | *p*-Value | Adj. *p*-Value |
|---|---|---|---|---|
| X(0 cm) vs. X(−10 cm) | 1.7778 | 1.9475 | 0.0515 | 0.5148 |
| X(0 cm) vs. X(−20 cm) | 2.4444 | 2.6778 | 0.0044 | 0.0441 * |
| X(0 cm) vs. X(−30 cm) | 2.0000 | 2.1909 | 0.0285 | 0.2846 |
| X(0 cm) vs. X(−40 cm) | 2.1111 | 2.3126 | 0.0207 | 0.2074 |
| X(−10 cm) vs. X(−20 cm) | 0.6667 | 0.7303 | 0.4652 | 1.0000 |
| X(−10 cm) vs. X(−30 cm) | 0.2222 | 0.2434 | 0.8077 | 1.0000 |
| X(−10 cm) vs. X(−40 cm) | 0.3333 | 0.3651 | 0.7150 | 1.0000 |
| X(−20 cm) vs. X(−30 cm) | −0.4444 | −0.4869 | 0.6264 | 1.0000 |
| X(−20 cm) vs. X(−40 cm) | −0.3333 | −0.3651 | 0.7150 | 1.0000 |
| X(−30 cm) vs. X(−40 cm) | 0.1111 | 0.1217 | 0.9031 | 1.0000 |

*: $p < 0.05$.

## 4. Discussion

### *4.1. Physicochemical Controls on Nutrient Ionic Activity in Intertidal Porewater*

As described earlier, the activity coefficients of all three ions declined slightly with depth because of increasing porewater salinity, reflecting ionic strength effects such as ion pairing [51,52]. Although these changes in activity coefficients were small, calculating activity remains important because it separates thermodynamic behavior from concentration-driven variations and clarifies the interpretation of vertical patterns.

The resulting activity profiles reflect both ionic strength effects and redox-driven changes. The redox conditions, such as oxic, suboxic, and anoxic, that are discussed in this study were not directly measured during our field study; instead, they are inferred from a well-known literature review of salty and brackish water environments. As shown in Figure 7, $NO_3^-$ activity increases with depth despite a slight decrease in the activity coefficient, indicating that concentration increases caused by diffusion or suboxic nitrification outweigh thermodynamic suppression. $NH_4^+$ shows a strong rise at depth (Figure 8), consistent with inhibited nitrification and enhanced ammonification under anoxic conditions. $PO_4^{3-}$ behaves differently: its activity peaks near −20 cm (Figure 9), suggesting potential release from Fe-bound phases near the redox boundary, and decreases again where sorption or precipitation dominates.

Figure 9 further indicates that ionic strength alone cannot explain nutrient mobility; redox-related changes in concentration interact with activity coefficients to produce the observed vertical patterns. Although seasonal porewater data were not fully collected, the pronounced geochemical transition observed around −20 cm is consistent with the freshwater–saltwater stratification typical of coastal tidal flats, where spring snowmelt, river discharge, and shallow groundwater inputs can overlie more saline, tidally influenced porewater. Therefore, despite the recurring shift in profiles around −20 cm and the statistical support, it should be interpreted cautiously as a potential transition zone but not as a well-defined interface.

#### 4.1.1. $NO_3^-$

The $NO_3^-$ activity coefficient decreased with depth in intertidal sediment porewater. As noted above, higher activity coefficients near the surface reflect the lower ionic strength of shallow porewater, and the decline at depth is consistent with the salinity-driven ionic strength increase discussed earlier [53]. Elevated salinity can suppress denitrification and promote $NO_3^-$ accumulation [54]. Although $NO_3^-$ activity slightly increased at depth,

concentrations were near the detection limit, and the trend should be interpreted cautiously. This reflects both ionic interactions and microbially driven redox processes in porewater.

#### 4.1.2. $NH_4^+$

The $NH_4^+$ activity coefficient followed a similar trend to that of $NO_3^-$, decreasing slightly from 0 to −40 cm (Figure 10). This trend follows the same ionic strength effect described above [55]. The increase in $NH_4^+$ activity with depth is consistent with salinity-enhanced release processes, as will be discussed later.

#### 4.1.3. $PO_4^{3-}$

As a trivalent anion, the $PO_4^{3-}$ activity coefficient shows greater sensitivity to ionic strength than monovalent ions and its activity coefficient decreased significantly. Near-surface conditions interpreted as oxic promote adsorption, as discussed in the $PO_4^{3-}$ dynamics section later. This implies that $PO_4^{3-}$ ions remain free in the medium, making them more mobile and increasing their activity coefficient. Another phenomenon involved is organic matter remineralization, which continuously supplies additional $PO_4^{3-}$ ions to the system. In deeper sediments, elevated salinity markedly increases ionic strength, strengthening electrostatic interactions and promoting counterion pairing. At depth, multiple processes, including complexation, adsorption–desorption shifts, and possible precipitation, collectively reduce the activity coefficient, as detailed later. The activity profiles indicate that a portion of the porewater $PO_4^{3-}$ pool becomes thermodynamically constrained as salinity increases with depth, due to the suppression of ionic activity relative to the measurable $PO_4^{3-}$ concentration. This implies that concentration alone may overestimate the chemically effective fraction of dissolved $PO_4^{3-}$ under high ionic strength conditions. Consequently, salinity-driven non-ideal behavior should be considered when interpreting porewater phosphate mobility in saline intertidal sediments.

### *4.2. Biogeochemical Processes Shaping Nutrient Profiles*

This study discusses salinity as a potential factor controlling nutrient non-ideal behavior through its physicochemical influence on ionic strength and activity coefficients, rather than through statistical inference. Although the statistical analysis revealed significant depth-dependent differences in salinity, temperature did not show statistically significant variation with depth. Importantly, the statistical significance of salinity alone does not imply causality in nutrient activity variability.

#### 4.2.1. N Dynamics

Biogeochemical processes in wetlands are closely linked to environmental conditions [56,57]. In this context, we analyze the effect of depth and salinity on nutrient activity coefficients and ionic activity in a medium of moderate ionic strength. As a result, tidal pumping in surface sediments generates pressure gradients between the overlying water column and the adjacent nutrient-rich sediment layers. The slight decrease in $NO_3^-$ and $NH_4^+$ activity coefficients reflects increasing ionic strength with depth. As noted earlier, a surface-inferred oxic layer promotes $NO_3^-$ adsorption to Fe/Al minerals. In the case of $NH_4^+$, nitrification processes carried out by nitrifying bacteria in the inferred oxic zone (surface sediments) convert $NH_4^+$ to $NO_3^-$ via potential redox reactions, thereby reducing $NH_4^+$ activity [58,59]. Ion exchange with clay minerals also reduces $NH_4^+$ concentrations at depth [60,61]. Clay minerals such as montmorillonite also influence $NH_4^+$ retention. In deep brackish sediments, an increase in ionic strength with depth can increase or decrease the actual nutrient concentration in porewater. Generally, in deep sediment assimilated to anoxic conditions, porewater $NO_3^-$ availability tends to decrease with increasing ionic strength due to microbial activity and the conversion of $NO_3^-$ to $NH_4^+$ [62]. Unexpectedly,

we observed the opposite behavior, as reported in some past studies, in which an increase in ionic strength led to a higher actual $NO_3^-$ concentration. However, the observed $NO_3^-$ increase in this study was very small and occurred at concentrations near the detection limit; therefore, this trend should be interpreted cautiously. High salinity inhibits microbial activity by reducing the denitrification rate; $NO_3^-$ removal performance is affected, thereby contributing to $NO_3^-$ accumulation if there are additional sources such as groundwater inflow from the overlying water [63,64]. The adsorption of $NO_3^-$ in mineral-rich sediments is also affected by ionic strength [65,66]. $NH_4^+$, on the other hand, is well documented to be released into the overlying water from deep sediment with increased ionic strength, thereby increasing its accumulation [21,67,68]—Figure 10. Continued $NH_4^+$ release can promote eutrophication and pose toxicity risks to aquatic biota [62].

#### 4.2.2. P Dynamics

The activity coefficient of $PO_4^{3-}$ is highest at the lowest ionic strength (0.61 mol/kg). However, it declines slightly with increasing depth and ionic strength while its activity rises, as shown in Figure 10c. This suggests that the $PO_4^{3-}$ ion interacts with porewater sediments, leading to depletion via adsorption. The adsorption of $PO_4^{3-}$ ions onto sediment surfaces can result in absorption through interactions with organic matter or the formation of new compounds, such as $Fe(PO_4)$ or $Fe_3(PO_4)_2$ and $Ca_3(PO_4)_2$, in an oxic environment. These processes influence $PO_4^{3-}$ mobility in sediments [69,70]. $PO_4^{3-}$ in deep sediment layers, influenced by factors such as ionic pairing, precipitation, redox reactions, and electrostatic ionic shielding occurring simultaneously or independently, impacts $PO_4^{3-}$ bioavailability [71] and alters its activity coefficient and activity. These combined deep sediment processes regulate $PO_4^{3-}$ bioavailability.

### *4.3. Comparative Insights from Other Intertidal Systems*

As reported in previous studies, deeper anoxic sediments commonly accumulate $NH_4^+$ and $PO_4^{3-}$ due to mineral dissolution, reductive processes, and suppressed denitrification [13,72]. Our findings for $NH_4^+$ are consistent with these mechanisms, whereas the phosphate profile diverges below −20 cm. A similar depth-dependent shift has been observed in the Janssand tidal flat, although our sediment shows a decline in phosphate activity below −20 cm. A previous study [73] also reported strong $NO_3^-$ depletion and $NH_4^+$ accumulation in brackish marsh sediments, consistent with our shallow-depth trends. However, the deeper decline in $PO_4^{3-}$ activity appears to be characteristic of this site's higher salinity and ionic strength gradients.

## 5. Conclusions

This study shows that depth-dependent changes in salinity and the resulting variation in ionic strength are the primary physicochemical drivers of nutrient mobility in the intertidal sediments of Lake Komuke. Assessing nutrients through activity and activity coefficients offers empirical constraints on how porewater nutrient behavior is understood in tidal flat systems. When ionic activity is explicitly accounted for in a concentrated environment, differences emerge between concentration- and ionic activity-based approaches, showing that even small changes in ionic strength can alter the thermodynamic behavior of dissolved nitrogen and phosphorus species. A distinct transition zone near −20 cm, marked by a clear increase in ionic strength, coincided with clear shifts in nutrient activity, particularly for $PO_4^{3-}$, whose strong sensitivity reflected ion–ion interactions and sediment geochemistry, resulting in a potential chemically constrained $PO_4^{3-}$ pool. These patterns highlight how nutrient mobility emerges from the combined influence of salinity gradients, inferred redox conditions, and mineral interactions. Overall, the findings indicate that

subsurface nutrient cycling in coastal tidal flats is shaped by the interplay of ionic strength and sediment geochemistry. While broader implications for carbon dynamics remain conceptual, the results offer baseline insights into nutrient regeneration and subsurface biogeochemical processes in northern intertidal systems. Future work with finer vertical resolution, multi-season sampling, and coupled transport modeling will be essential to fully resolve the thermodynamic controls governing nutrient transformations.

**Supplementary Materials:** The following supporting information can be downloaded at: https://www.mdpi.com/article/10.3390/environments13020117/s1, Figure S1: Monthly variations in salinity and temperature at different sediment depths; Figure S2: Monthly variations in porewater concentrations of (a) $NO_3^-$, (b) $NH_4^+$, and (c) $PO_4^{3-}$ at different sediment depths; Figure S3: Monthly variations in porewater concentrations correlated with activity of $NO_3^-$ across stations; Figure S4: Monthly variations in porewater concentrations correlated with activity of $NH_4^+$ across stations; Figure S5: Monthly variations in porewater concentrations correlated with activity of $PO_4^{3-}$ across stations.

**Author Contributions:** A.M.S. and K.K.: conceptualization and methodology. A.M.S.: software, validation, formal analysis, and investigation. K.K.: resources. A.M.S.: data curation and writing—original draft preparation. A.M.S. and K.K.: writing—review and editing and visualization. K.K.: supervision. A.M.S. and K.K.: funding acquisition. All authors have read and agreed to the published version of the manuscript.

**Funding:** The field observations used in this study were conducted with the support of the Grant-in-Aid for Scientific Research (C) from the Japan Society for the Promotion of Science (JSPS), Project No. 21H05178, Project No. 15K00514, entitled "Improvement of environmental dynamics analysis of river basin using specific substance information in cold region." The first author, Abdoulkader Moussa Siddo, was financially supported by the JICA SDGs Global Leader Program during his doctoral studies at the Kitami Institute of Technology, Japan.

**Data Availability Statement:** The original contributions presented in this study are included in the article. For further inquiries, please contact the corresponding author.

**Acknowledgments:** Part of the dataset used in this study was obtained from field and laboratory work conducted in 2016 by T. Takeuchi, a former student of Kitami Institute of Technology, to whom the authors express their sincere appreciation.

**Conflicts of Interest:** The authors declare no conflicts of interest.

## Appendix A

The Pitzer formulation accounts for binary and ternary ion interactions and is widely applied to natural waters with elevated salinity.

$$ln\gamma_i = D.H.L.L + \sum_{ij} m_i m_j B_{ij}^{\gamma} + \sum_{ijk} m_i m_j m_k C_{ijk}^{\gamma} \quad \text{(A1)}$$

where D.H.L.L stands for the Debye–Hückel limiting law, which is a function of ionic strength; $m_i$, $m_j$, $m_k$ are the molality of the cation and anion; $B_{ij}^{\gamma}$ is the parameters of binary interactions between the cation and anion; $C_{ijk}^{\gamma}$ is the parameters of ternary interactions between two cations and one anion or two anions and one cation; and $\gamma_i$ is the individual ion activity coefficient.

$$f^{\gamma} = -0.392\left[\frac{I^{\frac{1}{2}}}{1+1.2I^{\frac{1}{2}}} + \frac{2}{1.2}\ln\left(1+1.2I^{\frac{1}{2}}\right)\right] \quad \text{(A2)}$$

where $f^{\gamma}$ represents the Debye–Hückel limiting law contribution and I is the ionic strength.

Our aim is to utilize the Pitzer equation because it accounts for concentrated solutions and interprets statistical results regarding the effect of salinity on ion species. This study does not aim to improve or modify the Pitzer model but rather to provide a straightforward application. The Pitzer equation is particularly relevant for examining the chemical particle behavior of natural waters, especially in concentrated solutions where salinity affects the medium ion species. For more detailed information about the Pitzer equation, one can refer to [48,49,74,75]. Furthermore, it is crucial to highlight certain aspects of the Pitzer equation, such as the activity coefficients associated with cations and anions in solution.

Equations (A4)–(A6) outline the activity coefficients for the ions $NO_3{}^-$, $NH_4{}^+$, and $PO_4{}^{3-}$, respectively. Conversely, they illustrate the interactions of these ions with principal ions, such as $K^+$ with $NO_3{}^-$, $N_a{}^+$ with $PO_4{}^{3-}$, and $SO_4{}^{2-}$ with $NH_4{}^+$. Equation (A3) presents the general form of the activity coefficient for natural water:

$$ln\gamma_i = Z^2 f^\gamma + IB_i^0 + f^1 B_i^1 + I^2 C_i \quad \text{(A3)}$$

where $f^1 = \left[1 - \exp\left(-2I^{\frac{1}{2}}\right)\left(1 + 2I^{\frac{1}{2}} - 2I\right)\right]$ and the coefficients $B_i^0$, $B_i^1$, and $C_i$ are determined from the values of $\beta^0$, $\beta^1$, and $C^\Theta$ for ions $NO_3{}^-$, $NH_4{}^+$, and $PO_4{}^{3-}$ in interstitial seawater of tidal flat. $B_i^0$, $B_i^1$, and $C_i$ were obtained for various ions from the work of [49,76].

$$ln\gamma_{NO_3^-} = Z^2_{NO_3^-} f^\gamma + 2I\left(B_{KNO_3} + IC_{KNO_3}\right) + I^2\left(Z^2_{NO_3^-} B^1_{KNO_3} + Z_{NO_3^-} C_{KNO_3}\right) \quad \text{(A4)}$$

$$ln\gamma_{PO_4^{3-}} = Z^2_{PO_4^{3-}} f^\gamma + 2I\left(B_{Na_3PO_4} + IC_{Na_3PO_4}\right) + I^2\left(Z^2_{PO_4^{3-}} B^1_{Na_3po_4} + Z_{PO_4^{3-}} C_{Na_3PO_4}\right) \quad \text{(A5)}$$

$$ln\gamma_{NH_4^+} = Z^2_{NH_4} f^\gamma + 2I\left(B_{(NH_4)_2SO_4} + IC_{(NH_4)_2SO_4}\right) + I^2\left(Z^2_{NH_4^+} B^1_{(NH_4)2SO_4} + Z_{NH_4^+} C_{(NH_4)2SO_4}\right) \quad \text{(A6)}$$

where $Z^2 f^\gamma$ is the Debye–Hückel limiting law part, I is the ionic strength, $Z$ is the valence of the ion, and B, $B^1$, and C are obtained from the general formulas as follows $B_{MX} = \beta^0_{MX} + \left(\frac{\beta^1_{MX}}{2I}\right)\left(1 - \left(1 + 2I^{\frac{1}{2}}\right)e^{-2I^{\frac{1}{2}}}\right)$, $B^1_{MX} = \left(\frac{\beta^1_{MX}}{2I^2}\right)\left(-1 + \left(1 + 2I^{\frac{1}{2}} + 2I\right)e^{-2I^{\frac{1}{2}}}\right)$, and $C_{MX} = \frac{C^\varnothing_{MX}}{2\,|\,Z_M Z_X\,|^{\frac{1}{2}}}$ and account for binary interactions.

## References


1. Murray, N.J.; Phinn, S.P.; Fuller, R.A.; DeWitt, M.; Ferrari, R.; Johnston, R.; Clinton, N.; Lyons, M.B. High-resolution global maps of tidal flat ecosystems from 1984 to 2019. *Sci. Data* **2022**, *9*, 542. [CrossRef] [PubMed]
2. Murray, N.J.; Phinn, S.R.; DeWitt, M.; Ferrari, R.; Johnston, R.; Lyons, M.B.; Clinton, N.; Thau, D.; Fuller, R.A. The global distribution and trajectory of tidal flats. *Nature* **2019**, *565*, 222–225. [CrossRef] [PubMed]
3. Murray, N.J.; Ma, Z.; Fuller, R.A. Tidal flats of the Y ellow S ea: A review of ecosystem status and anthropogenic threats. *Austral. Ecol.* **2015**, *40*, 472–481. [CrossRef]
4. Zhou, Z.; Grandjean, T.J.; de Smit, J.; van Belzen, J.; Fivash, G.S.; Walles, B.; Beauchard, O.; van Dalen, J.; Blok, D.B.; van IJzerloo, L. Sediment dynamics shape macrofauna mobility traits and abundance on tidal flats. *Limnol. Oceanogr.* **2024**, *69*, 2278–2293. [CrossRef]
5. Reise, K. *Tidal Flat Ecology: An Experimental Approach to Species Interactions*; Springer Science & Business Media: Berlin/Heidelberg, Germany, 2012; Volume 54.
6. Beck, M.; Brumsack, H.-J. Biogeochemical cycles in sediment and water column of the Wadden Sea: The example Spiekeroog Island in a regional context. *Ocean Coast. Manag.* **2012**, *68*, 102–113. [CrossRef]
7. Zhang, Y.; Xiao, X.; Sun, Z.; Lei, B.; Li, M.; Guo, X.; Fu, T.; Xing, C. Salt dynamic changes between seawater and phreatic brine in muddy tidal flats under tidal influence. *J. Hydrol.* **2024**, *634*, 131044. [CrossRef]
8. Li, Y.; Pan, D. Empirical Orthogonal Function Analysis on Long-Term Profile Evolution of Tidal Flats along a Curved Coast in the Qiantang River Estuary, China. *J. Mar. Sci. Eng.* **2024**, *12*, 1089. [CrossRef]

9. Anschutz, P.; Smith, T.; Mouret, A.; Deborde, J.; Bujan, S.; Poirier, D.; Lecroart, P. Tidal sands as biogeochemical reactors. *Estuar. Coast. Shelf Sci.* **2009**, *84*, 84–90. [CrossRef]
10. Schutte, C.; Ahmerkamp, S.; Wu, C.S.; Seidel, M.; De Beer, D.; Cook, P.; Joye, S.B. Biogeochemical dynamics of coastal tidal flats. In *Coastal Wetlands*; Elsevier: Amsterdam, The Netherlands, 2019; pp. 407–440.
11. Reckhardt, A.; Beck, M.; Seidel, M.; Riedel, T.; Wehrmann, A.; Bartholomä, A.; Schnetger, B.; Dittmar, T.; Brumsack, H.-J. Carbon, nutrient and trace metal cycling in sandy sediments: A comparison of high-energy beaches and backbarrier tidal flats. *Estuar. Coast. Shelf Sci.* **2015**, *159*, 1–14. [CrossRef]
12. Dung, L.V.; Tue, N.T.; Quy, T.D.; Nhuan, M.T. Ammonium, Nitrate, and Phosphate in Coastal Waters of Red River Biosphere Reserve, Vietnam: 10.32526/ennrj/23/20240128. *Environ. Nat. Resour. J.* **2025**, *23*, 55–64. [CrossRef]
13. Beck, M.; Reckhardt, A.; Amelsberg, J.; Bartholomä, A.; Brumsack, H.-J.; Cypionka, H.; Dittmar, T.; Engelen, B.; Greskowiak, J.; Hillebrand, H. The drivers of biogeochemistry in beach ecosystems: A cross-shore transect from the dunes to the low-water line. *Mar. Chem.* **2017**, *190*, 35–50. [CrossRef]
14. Xie, R.; Rao, P.; Pang, Y.; Shi, C.; Li, J.; Shen, D. Salt intrusion alters nitrogen cycling in tidal reaches as determined in field and laboratory investigations. *Sci. Total Environ.* **2020**, *729*, 138803. [CrossRef] [PubMed]
15. Rysgaard, S.; Thastum, P.; Dalsgaard, T.; Christensen, P.B.; Sloth, N.P. Effects of salinity on NH4+ adsorption capacity, nitrification, and denitrification in Danish estuarine sediments. *Estuaries* **1999**, *22*, 21–30. [CrossRef]
16. Herbert, R. Nitrogen cycling in coastal marine ecosystems. *FEMS Microbiol. Rev.* **1999**, *23*, 563–590. [CrossRef] [PubMed]
17. Zhang, G.; Bai, J.; Zhai, Y.; Jia, J.; Zhao, Q.; Wang, W.; Hu, X. Microbial diversity and functions in saline soils: A review from a biogeochemical perspective. *J. Adv. Res.* **2024**, *59*, 129–140. [CrossRef]
18. Li, X.; Wang, A.; Wan, W.; Luo, X.; Zheng, L.; He, G.; Huang, D.; Chen, W.; Huang, Q. High salinity inhibits soil bacterial community mediating nitrogen cycling. *Appl. Environ. Microbiol.* **2021**, *87*, e01366-21. [CrossRef]
19. Bouvier, T.C.; del Giorgio, P.A. Compositional changes in free-living bacterial communities along a salinity gradient in two temperate estuaries. *Limnol. Oceanogr.* **2002**, *47*, 453–470. [CrossRef]
20. Tully, K.; Gedan, K.; Epanchin-Niell, R.; Strong, A.; Bernhardt, E.S.; BenDor, T.; Mitchell, M.; Kominoski, J.; Jordan, T.E.; Neubauer, S.C. The invisible flood: The chemistry, ecology, and social implications of coastal saltwater intrusion. *BioScience* **2019**, *69*, 368–378. [CrossRef]
21. Herbert, E.R.; Boon, P.; Burgin, A.J.; Neubauer, S.C.; Franklin, R.B.; Ardón, M.; Hopfensperger, K.N.; Lamers, L.P.; Gell, P. A global perspective on wetland salinization: Ecological consequences of a growing threat to freshwater wetlands. *Ecosphere* **2015**, *6*, 1–43. [CrossRef]
22. Millero, F.; Pierrot, D. Speciation of metals in natural waters. *Chem. Mar. Water Sediments* **2002**, *2*, 57. [CrossRef]
23. Millero, F. Physicochemical Controls. In *Marine Geochemistry*; CRC Press: Boca Raton, FL, USA, 2006; Chapter 6.
24. Pitzer, K.S. Electrolyte theory-improvements since Debye and Hueckel. *Acc. Chem. Res.* **1977**, *10*, 371–377. [CrossRef]
25. Zhang, J.-Z.; Huang, X.-L. Effect of temperature and salinity on phosphate sorption on marine sediments. *Environ. Sci. Technol.* **2011**, *45*, 6831–6837. [CrossRef] [PubMed]
26. Sundareshwar, P.; Morris, J.T. Phosphorus sorption characteristics of intertidal marsh sediments along an estuarine salinity gradient. *Limnol. Oceanogr.* **1999**, *44*, 1693–1701. [CrossRef]
27. Bååth, E.; Kritzberg, E.S. Temperature Adaptation of Aquatic Bacterial Community Growth Is Faster in Response to Rising than to Falling Temperature. *Microb. Ecol.* **2024**, *87*, 38. [CrossRef] [PubMed]
28. Kirwan, M.L.; Guntenspergen, G.R.; Langley, J. Temperature sensitivity of organic-matter decay in tidal marshes. *Biogeosciences* **2014**, *11*, 4801–4808. [CrossRef]
29. Valdemarsen, T.; Quintana, C.O.; Flindt, M.R.; Kristensen, E. Organic N and P in eutrophic fjord sediments–rates of mineralization and consequences for internal nutrient loading. *Biogeosciences* **2015**, *12*, 1765–1779. [CrossRef]
30. Verhamme, D.T.; Prosser, J.I.; Nicol, G.W. Ammonia concentration determines differential growth of ammonia-oxidising archaea and bacteria in soil microcosms. *ISME J.* **2011**, *5*, 1067–1071. [CrossRef]
31. de Klein, J.J.; Overbeek, C.C.; Juncher Jørgensen, C.; Veraart, A.J. Effect of temperature on oxygen profiles and denitrification rates in freshwater sediments. *Wetlands* **2017**, *37*, 975–983. [CrossRef]
32. Haas, S.; Robicheau, B.M.; Rakshit, S.; Tolman, J.; Algar, C.K.; LaRoche, J.; Wallace, D.W. Physical mixing in coastal waters controls and decouples nitrification via biomass dilution. *Proc. Natl. Acad. Sci. USA* **2021**, *118*, e2004877118. [CrossRef]
33. Pajares, S.; Ramos, R. Processes and microorganisms involved in the marine nitrogen cycle: Knowledge and gaps. *Front. Mar. Sci.* **2019**, *6*, 739. [CrossRef]
34. Schutte, C.A.; Wilson, A.M.; Evans, T.; Moore, W.S.; Joye, S.B. Deep oxygen penetration drives nitrification in intertidal beach sands. *Limnol. Oceanogr.* **2018**, *63*, S193–S208. [CrossRef]
35. Boström, B.; Andersen, J.M.; Fleischer, S.; Jansson, M. Exchange of Phosphorus Across the Sediment-Water Interface. In *Proceedings of the Phosphorus in Freshwater Ecosystems: Proceedings of a Symposium Held in Uppsala, Sweden, 25–28 September 1985*; Springer: Berlin/Heidelberg, Germany, 1988.

36. Santos, I.R.; Bryan, K.R.; Pilditch, C.A.; Tait, D.R. Influence of porewater exchange on nutrient dynamics in two New Zealand estuarine intertidal flats. *Mar. Chem.* **2014**, *167*, 57–70. [CrossRef]
37. Wang, F.; Xiao, K.; Santos, I.R.; Lu, Z.; Tamborski, J.; Wang, Y.; Yan, R.; Chen, N. Porewater exchange drives nutrient cycling and export in a mangrove-salt marsh ecotone. *J. Hydrol.* **2022**, *606*, 127401. [CrossRef]
38. Ardila, P.A.R.; Alonso, R.Á.; Valsero, J.J.D.; García, R.M.; Cabrera, F.Á.; Cosío, E.L.; Laforet, S.D. Assessment of heavy metal pollution in marine sediments from southwest of Mallorca island, Spain. *Environ. Sci. Pollut. Res.* **2023**, *30*, 16852–16866. [CrossRef]
39. Garcia-Robledo, E.; Bohorquez, J.; Corzo, A.; Jimenez-Arias, J.L.; Papaspyrou, S. Dynamics of inorganic nutrients in intertidal sediments: Porewater, exchangeable, and intracellular pools. *Front. Microbiol.* **2016**, *7*, 761. [CrossRef]
40. Froelich, P.; Arthur, M.; Burnett, W.; Deakin, M.; Hensley, V.; Jahnke, R.; Kaul, L.; Kim, K.-H.; Roe, K.; Soutar, A. Early diagenesis of organic matter in Peru continental margin sediments: Phosphorite precipitation. *Mar. Geol.* **1988**, *80*, 309–343. [CrossRef]
41. Handler, E.R.; Andersen, S.D.; Gradinger, R.; McGovern, M.; Vader, A.; Poste, A.E. Seasonality in land–ocean connectivity and local processes control sediment bacterial community structure and function in a High Arctic tidal flat. *FEMS Microbiol. Ecol.* **2024**, *100*, fiad162. [CrossRef]
42. Yu, X.; Xu, X.; Zhan, L.; Cheng, H.; Xin, P. Seasonal temperature distributions and variations in salt marshes: Field investigation and numerical simulation. *Water Resour. Res.* **2024**, *60*, e2023WR037016. [CrossRef]
43. Waska, H.; Greskowiak, J.; Ahrens, J.; Beck, M.; Ahmerkamp, S.; Böning, P.; Brumsack, H.; Degenhardt, J.; Ehlert, C.; Engelen, B. Spatial and temporal patterns of pore water chemistry in the inter-tidal zone of a high energy beach. *Front. Mar. Sci.* **2019**, *6*, 154. [CrossRef]
44. Friedman, M. The use of ranks to avoid the assumption of normality implicit in the analysis of variance. *J. Am. Stat. Assoc.* **1937**, *32*, 675–701. [CrossRef]
45. Ferguson, C.A. The structure and use of politeness formulas. *Lang. Soc.* **1976**, *5*, 137–151. [CrossRef]
46. Dickson, A.G.; Goyet, C. *Handbook of Methods for the Analysis of the Various Parameters of the Carbon Dioxide System in Sea Water, Version 2*; Oak Ridge National Lab (ORNL): Oak Ridge, TN, USA, 1994.
47. Meija, J.; Coplen, T.B.; Berglund, M.; Brand, W.A.; De Bièvre, P.; Gröning, M.; Holden, N.E.; Irrgeher, J.; Loss, R.D.; Walczyk, T. Atomic weights of the elements 2013 (IUPAC Technical Report). *Pure Appl. Chem.* **2016**, *88*, 265–291. [CrossRef]
48. Pitzer, K.S. Thermodynamics of electrolytes. I. Theoretical basis and general equations. *J. Phys. Chem.* **1973**, *77*, 268–277. [CrossRef]
49. Millero, F.J.; Pierrot, D. A chemical equilibrium model for natural waters. *Aquat. Geochem.* **1998**, *4*, 153–199. [CrossRef]
50. Pierrot, D.; Millero, F.J. The speciation of metals in natural waters. *Aquatic Geochem.* **2017**, *23*, 1–20. [CrossRef]
51. Valiskó, M.; Boda, D. Unraveling the behavior of the individual ionic activity coefficients on the basis of the balance of ion–ion and ion–water interactions. *J. Phys. Chem. B* **2015**, *119*, 1546–1557. [CrossRef]
52. Ferse, A. Numerical values of individual activity coefficients of single-ion species in concentrated aqueous electrolyte solutions and the attempt of a qualitative interpretation on a model of electrostatic interaction. *J. Solid State Electrochem.* **2013**, *17*, 1321–1332. [CrossRef]
53. Qasem, N.A.; Generous, M.M.; Qureshi, B.A.; Zubair, S.M. A comprehensive review of saline water correlations and data: Part II—Thermophysical properties. *Arab. J. Sci. Eng.* **2021**, *46*, 1941–1979. [CrossRef]
54. Luo, Z.; Kong, J.; Yu, X.; Gao, C.; Barry, D.; Fatichi, S. Seawater intrusion inhibits nitrate removal in tidal marsh aquifers. *Water Resour. Res.* **2024**, *60*, e2024WR038107. [CrossRef]
55. Yin, H.; Zhu, J.; Tang, W. Management of nitrogen and phosphorus internal loading from polluted river sediment using Phoslock® and modified zeolite with intensive tubificid oligochaetes bioturbation. *Chem. Eng. J.* **2018**, *353*, 46–55. [CrossRef]
56. Rezanezhad, F.; McCarter, C.P.; Lennartz, B. Wetland biogeochemistry: Response to environmental change. *Front. Environ. Sci.* **2020**, *8*, 55. [CrossRef]
57. Reddy, K.R.; DeLaune, R.D.; Inglett, P.W. *Biogeochemistry of Wetlands: Science and Applications*; CRC Press: Boca Raton, FL, USA, 2022.
58. Zhao, R.; Mogollón, J.M.; Roerdink, D.L.; Thorseth, I.H.; Økland, I.; Jørgensen, S.L. Ammonia-oxidizing archaea have similar power requirements in diverse marine oxic sediments. *ISME J.* **2021**, *15*, 3657–3667. [CrossRef] [PubMed]
59. Wankel, S.D.; Mosier, A.C.; Hansel, C.M.; Paytan, A.; Francis, C.A. Spatial variability in nitrification rates and ammonia-oxidizing microbial communities in the agriculturally impacted Elkhorn Slough estuary, California. *Appl. Environ. Microbiol.* **2011**, *77*, 269–280. [CrossRef] [PubMed]
60. Alshameri, A.; He, H.; Zhu, J.; Xi, Y.; Zhu, R.; Ma, L.; Tao, Q. Adsorption of ammonium by different natural clay minerals: Characterization, kinetics and adsorption isotherms. *Appl. Clay Sci.* **2018**, *159*, 83–93. [CrossRef]
61. Zhang, C.; Tang, H.; Abdulgawad, F.; Bockelmann, E.B.; Sapsford, D.; Williams, K.; Falconer, R. Ammonium Ion Adsorption on Clays and Sand Under Freshwater and Seawater Conditions. In *Advances in Water Resources and Hydraulic Engineering: Proceedings of 16th IAHR-APD Congress and 3rd Symposium of IAHR-ISHS*; Springer: Berlin/Heidelberg, Germany, 2009.

62. Zheng, H.; Yin, Z.; Chen, L.; He, H.; Li, Z.; Lv, X.; Chen, J.; Du, W.; Lin, X. Effects of salinity on nitrogen reduction pathways in estuarine wetland sediments. *Mar. Pollut. Bull.* **2024**, *207*, 116834. [CrossRef]
63. Luo, Z.; Zhong, Q.; Han, X.; Hu, R.; Liu, X.; Xu, W.; Wu, Y.; Huang, W.; Zhou, Z.; Zhuang, W. Depth-dependent variability of biological nitrogen fixation and diazotrophic communities in mangrove sediments. *Microbiome* **2021**, *9*, 212. [CrossRef]
64. Whitfield, A.K.; Wood, A.D. *Studies on the River-Estuary Interface Region of Selected Eastern Cape Estuaries*; Water Research Commission: Pretoria, South Africa, 2003.
65. Donn, M.; Menzies, N. The effect of ionic strength variation and anion competition on the development of nitrate accumulations in variable charge subsoils. *Soil Res.* **2005**, *43*, 43–50. [CrossRef]
66. Wang, F.; Chen, N.; Yan, J.; Lin, J.; Guo, W.; Cheng, P.; Liu, Q.; Huang, B.; Tian, Y. Major processes shaping mangroves as inorganic nitrogen sources or sinks: Insights from a multidisciplinary study. *J. Geophys. Res. Biogeosciences* **2019**, *124*, 1194–1208. [CrossRef]
67. Gonzalez-Salgado, I.; Bounouba, M.; Dubos, S.; Mengelle, E.; Guigui, C.; Sperandio, M. Influence of feed salinity on ammonia recovery from high-strength effluents in transmembrane chemical absorption process. *J. Membr. Sci.* **2023**, *687*, 122086. [CrossRef]
68. Feder, R.C.; White, J.R. Impact of freshwater river reconnection on porewater salinity and ammonium availability in coastal brackish marsh soils. *Sci. Total Environ.* **2024**, *926*, 172131. [CrossRef]
69. Basinski, J.J.; Bone, S.E.; Klein, A.R.; Thongsomboon, W.; Mitchell, V.; Shukle, J.T.; Druschel, G.K.; Thompson, A.; Aristilde, L. Unraveling iron oxides as abiotic catalysts of organic phosphorus recycling in soil and sediment matrices. *Nat. Commun.* **2024**, *15*, 5930. [CrossRef]
70. Gomez, E.; Durillon, C.; Rofes, G.; Picot, B. Phosphate adsorption and release from sediments of brackish lagoons: pH, O2 and loading influence. *Water Res.* **1999**, *33*, 2437–2447. [CrossRef]
71. Parsons, C.T.; Rezanezhad, F.; O'Connell, D.W.; Van Cappellen, P. Sediment phosphorus speciation and mobility under dynamic redox conditions. *Biogeosciences* **2017**, *14*, 3585–3602. [CrossRef]
72. Howes, B.; Teal, J. Oxygen loss from Spartina alterniflora and its relationship to salt marsh oxygen balance. *Oecologia* **1994**, *97*, 431–438. [CrossRef] [PubMed]
73. Feder, R.C. Effects of Coastal Freshening on Porewater Salinity and Nitrogen Cycling in Brackish Marsh Soils: Implications for Biogeochemical Resilience in Barataria Basin, LA. Master's Thesis, Louisiana State University and Agricultural & Mechanical College, Baton Rouge, LA, USA, 2023.
74. Millero, F. Use of models to determine ionic interactions in natural waters. *Thalass. Jugosl.* **1982**, *18*, 253–291. [CrossRef]
75. Millero, F.J.; Ricco, J.; Schreiber, D.R. PVT properties of concentrated aqueous electrolytes. II. Compressibilities and apparent molar compressibilities of aqueous NaCl, Na 2 SO 4, MgCl 2, and MgSO 4 from dilute solution to saturation and from 0 to 50° C. *J. Solut. Chem.* **1982**, *11*, 671–686. [CrossRef]
76. Pitzer, K.S.; Kim, J.J. Thermodynamics of electrolytes. IV. Activity and osmotic coefficients for mixed electrolytes. *J. Am. Chem. Soc.* **1974**, *96*, 5701–5707. [CrossRef]


**Disclaimer/Publisher's Note:** The statements, opinions and data contained in all publications are solely those of the individual author(s) and contributor(s) and not of MDPI and/or the editor(s). MDPI and/or the editor(s) disclaim responsibility for any injury to people or property resulting from any ideas, methods, instructions or products referred to in the content.